Brain Struct Funct (2010) 214:375–393
DOI 10.1007/s00429-010-0239-z

ORIGINAL ARTICLE

The entorhinal cortex of the Megachiroptera: a comparative study of Wahlberg's epauletted fruit bat and the straw-coloured fruit bat

Catherine W. Gatome · Lutz Slomianka · Dieter K. Mwangi · Hans-Peter Lipp · Irmgard Amrein

Received: 16 October 2009 / Accepted: 9 January 2010 / Published online: 4 February 2010

Abstract This study describes the organisation of the entorhinal cortex of the Megachiroptera, straw-coloured fruit bat and Wahlberg's epauletted fruit bat. Using Nissl and Timm stains, parvalbumin and SMI-32 immunohistochemistry, we identified five fields within the medial (MEA) and lateral (LEA) entorhinal areas. MEA fields E_{CL} and E_C are characterised by a poor differentiation between layers II and III, a distinct layer IV and broad, stratified layers V and VI. LEA fields E_I, E_R and E_L are distinguished by cell clusters in layer II, a clear differentiation between layers II and III, a wide columnar layer III and a broad sublayer Va. Clustering in LEA layer II was more typical of the straw-coloured fruit bat. Timm-staining was most intense in layers Ib and II across all fields and layer III of field E_R. Parvalbumin-like staining varied along a medio-lateral gradient with highest immunoreactivity in layers II and III of MEA and more lateral fields of LEA. Sparse SMI-32-like immunoreactivity was seen only in Wahlberg's epauletted fruit bat. Of the neurons in MEA layer II, ovoid stellate cells account for ~38%, polygonal stellate cells for ~8%, pyramidal cells for ~18%, oblique pyramidal cells for ~6% and other neurons of variable morphology for ~29%. Differences between bats and other species in cellular make-up and cytoarchitecture of layer II may relate to their three-dimensional habitat. Cytoarchitecture of layer V in conjunction with high encephalisation and structural changes in the hippocampus suggest similarities in efferent hippocampal → entorhinal → cortical interactions between fruit bats and primates.

Keywords *Epomophorus wahlbergi* · *Eidolon helvum* · Parvalbumin · SMI-32 · Timm-staining · Stereology

Abbreviations

EC	Entorhinal cortex
MEA	Medial entorhinal cortex
LEA	Lateral entorhinal cortex
PrS	Presubiculum
PaS	Parasubiculum
PRh	Perirhinal cortex
POR	Postrhinal cortex
PPC	Prepiriform cortex
E_{CL}	Caudal-limiting entorhinal field
E_C	Caudal entorhinal field
E_I	Intermediate entorhinal field
E_L	Lateral entorhinal field
E_R	Rostral entorhinal field

Introduction

Although detailed descriptions of the entorhinal cortex (EC) are available for most of the common species used in neuroscience research, they comprise only a small segment of the mammalian radiation. To our knowledge, no contemporary descriptions are available for one of the most species-rich mammalian orders, the Chiroptera. The few available studies date back to the beginning of the twentieth century. Rose (1912) described this region as bearing a strong semblance to the EC of other mammals. Brodmann

C. W. Gatome · L. Slomianka · H.-P. Lipp · I. Amrein (✉)
Institute of Anatomy, University of Zurich,
Winterthurerstrasse 190, 8057 Zurich, Switzerland
e-mail: i.amrein@anatom.uzh.ch

D. K. Mwangi
Department of Veterinary Anatomy and Physiology,
University of Nairobi, PO Box 30197, Nairobi 00100, Kenya

(1925) identified a medial and lateral subdivision in a megachiropteran species, *Pteropus edwardsi*. Later, Rose (1926) in his study of a microchiropteran species, *Vesperugo pipistrellus*, identified an additional subdivision, which he named area entorhinalis intermedia. In recognising only the medial and lateral entorhinal areas, early works generally do not conform to the parcellation of the EC developed more recently in other species. Buhl and Dann (1991) traced entorhinal afferents to the hippocampus in two megachiropteran species, but lacked information on the entorhinal fields, and therefore could not draw conclusions on topographical organisation of the entorhinal–hippocampal connections. Here, we provide a description of the EC in Megachiroptera (fruit bats), which is comparable with the parcellation that has been derived from recent cytoarchitectural and connectional studies in other species. The inclusion of two closely related species, Wahlberg's epauletted fruit bat (*Epomophorus wahlbergi*) and the straw-coloured fruit bat (*Eidolon helvum*), was prompted by perceptible differences between the species in the EC.

While the debate on the phylogenetics of the Chiroptera lingers on, the argument for a common ancestor of the Megachiroptera and primates (Maseko and Manger 2007; Pettigrew et al. 1989, 2008), and hence a diphyletic origin of the Mega- and Microchiroptera, has been weakened by mounting evidence from recent molecular phylogenetic analyses (Jones and Teeling 2006; Teeling et al. 2000). These favour a monophyletic origin of the two chiropteran suborders (Simmons et al. 2008). That notwithstanding, the Megachiroptera do share a number of brain characteristics with primates (Johnson et al. 1994; Lapointe et al. 1999). Of the analysed characters, most are related to the visual system. The Megachiroptera have a distinctly primate-like retinotectal pathway; retinal input into the midbrain is decussated so that only the contralateral hemifield is represented. The location of the lateral geniculate nucleus magnocellular layers adjacent to the optic tract and the presence of a middle temporal visual area are characteristics only described in the primates, Megachiroptera and Dermoptera (Pettigrew et al. 1989). More recently, features of the cholinergic, catecholaminergic and serotonergic systems were found to exhibit many similarities to those in primates (Maseko et al. 2007). A general evolutionary trend of the megachiropteran brain has been the enlargement of the telencephalon, most notably the neocortex—a trend which is also seen in primates (Baron et al. 1996b). Several cytoarchitectural characteristics of the hippocampus also resemble that of primates (Buhl and Dann 1991; Rosene and Van Hoesen 1987). Considering the similarities in brain structure, the Megachiroptera may present a small mammal model for investigating primate-like neural phenomena.

In the rat and mouse, grid cells have been described in layers II and III of the dorsocaudal region of the medial EC (Fyhn et al. 2008; Fyhn et al. 2004). Metric information is integrated in the entorhinal cortex by the grid and head-direction cells and fed to the hippocampal place cells (Jeffery 2007; Moser et al. 2008; O'Keefe and Burgess 2005). Place cells have recently been described in moving echolocating bats (Ulanovsky and Moss 2007), and it is probable that they are also modulated by grid cells. Bats may offer the possibility to study the spatial firing properties of the grid cells in three-dimensions. The specific neuronal phenotype of grid cells has not been identified. Physiological characterisation of the possible phenotypes has focused on the classical stellate and pyramidal cell (Alonso and Klink 1993). Based on morphology, our study estimates the relative contribution of neuronal phenotypes to the cell population of layer II.

Materials and methods

Animals

Wahlberg's epauletted fruit bats were captured in Nairobi, Kenya, and straw-coloured fruit bats were captured in Kampala, Uganda. Permits and licences were granted by the National Museums of Kenya and the Uganda National Council of Science and Technology (No. 024/07/1). The animals were aged as adults based on the following criteria: closure of the femoral and humeral epiphyseal plate, body weight above 60 g (Wahlberg's epauletted fruit bat) or 200 g (straw-coloured fruit bat), forearm length over 70 mm (Wahlberg's epauletted fruit bat) or 110 mm (straw-coloured fruit bat) and sexual maturity (evidence of lactation or pregnancy). The actual ages of the animals are not known, although individuals of this family have lived in captivity for over 20 years (Kingdon 1984).

Four adult female animals of each species were used in this study (straw-coloured fruit bat: mean body weight 267 g, mean brain weight 4.0 g; Wahlberg's epauletted fruit bat: mean body weight 82 g, mean brain weight 1.9 g).

Histology

Tissue preparation

Animals were deeply anaesthetized with sodium pentobarbital (Nembutal®, 60 mg/ml; 50 mg/kg) and transcardially perfused first with heparinised 0.9% saline, followed by 0.6% sodium sulphide solution and then cold 4% paraformaldehyde in 0.1 M phosphate buffer with 15% picric acid. Brains were removed and postfixed overnight at 4°C in fixative and then transferred to 30% sucrose for 24 h. The right hemisphere was processed for immunohistochemistry,

while the left hemisphere was embedded in glycolmethylacrylate (see below).

Immunohistochemistry

Staining batches always contained sections of both species. Antibody concentrations that gave the best signal to background ratio were determined by dilution series.

Forty-micron sections in the coronal plane were cut into 12 series using a cryotome. Sections from three series were rinsed in tris–triton buffer (pH 7.4), pretreated in 0.6% hydrogen peroxide, rinsed and preincubated in normal goat serum for 1 h. Two series were incubated for two nights with SMI-32 monoclonal antibody (1:5,000, SMI-32R Sternberger Monoclonals Inc., Maryland, USA) and one series with monoclonal anti-parvalbumin antibody (1:30,000, P-3171, Sigma, Missouri, USA). This was followed by rinsing with tris buffer (pH 7.4), incubation at room temperature for 2 h with biotinylated goat anti-mouse immunoglobulin (1:1,000, Vectastain® Elite ABC Kit, Vector Laboratories Inc, California, USA) and incubation for 35 min with avidin–biotin–peroxidase complex (Vectastain® Elite ABC Kit). Immunoreaction was detected using diaminobenzidine staining. Sections from one SMI 32-immunostained series were counterstained with Giemsa solution (see below).

The monoclonal anti-parvalbumin (mouse IgG1 isotype) used is derived from the PARV-19 hybridoma cells. Purified frog muscle was used as the immunogen. The antibody reacts with parvalbumin of human, bovine, goat, pig, rabbit, dog, cat, rat, frog and fish (Sigma, Missouri, USA). The monoclonal anti-SMI-32 is derived from mouse ascites fluid. Homogenised hypothalami of rats were used as the immunogen. The antibody reacts with a non-phosphorylated epitope in neurofilament H (180 and 200 kDa) of most mammalian species (Sternberger Monoclonals Inc., Maryland, USA).

The immunoreactive structures corresponded in appearance and general distribution to those observed in other mammalian species. However, as we cannot be certain of the epitope(s) recognised by the antibodies in the bat, we refer to the observed immunoreactivity as parvalbumin- and SMI-32-like.

To control for non-specific staining related to the secondary antibodies and avidin–biotin–peroxidase labelling, controls from each species, in which the primary antibody was omitted, was included in the experiment.

Nissl and Timm staining

Brains were dehydrated in ethanol (70% × 5 h, 96% × 5 h, 100% × 48 h), infiltrated in four changes (24 h, 3 days, 1 week, 1 week) of glycolmethylacrylate solution (Technovit 7100, Kulzer GmbH, Wehrheim, Germany) and embedded. Twenty micron horizontal sections were cut, and every sixth section was mounted and dried for 1 h at 60°C. Sections were stained with Giemsa solution (Merck, Darmstadt, Germany) diluted 1:10 in 0.07 M KH_2PO_4 buffer at room temperature for 1 h (Iñiguez et al. 1985). They were then differentiated for 10 s in 1% acetic acid followed by 10 s in 96% ethanol. Sections were dehydrated in two changes of absolute ethanol, cleared and coverslipped.

A second series was developed in Timm's solution prepared from a mixture of 120 ml gum arabic solution (50% weight/volume in distilled water), 20 ml citrate buffer solution (pH 5), 60 ml of 0.5% hydroquinone solution and 1 ml of 17% silver nitrate solution. After 3-h incubation at 37°C, the slides were rinsed in tap water, fixed for 1 min with 1% sodium thiosulfate and then dehydrated, cleared and coverslipped.

MEA layer II cell numbers and size

Layer II of medial entorhinal cortex was delineated on 20 μm glycolmethylacrylate-embedded Nissl-stained horizontal sections. Using the StereoInvestigator® software (MicroBrightfield Inc, Colchester, Vermont, USA), total cell numbers were estimated using the Optical Fractionator (West et al. 1991) with a 40 × oil-immersion objective (N.A. 1.3) in every 6th (Wahlberg's epauletted fruit bat) or 12th (straw-coloured fruit bat) section with a counting frame of 40 μm × 40 μm, a disector height of 10 μm and *x*, *y*-steps of 100 μm. Section thickness was measured at every sixth sampling site. Cell numbers were estimated using number-weighed section thickness (Dorph-Petersen et al. 2001). The nucleolus was used as the counting unit and also as a reference point for the Nucleator estimates (see below). We did not observe neuronal nuclei with more than one nucleolus.

The areas of cell profiles were estimated using the Nucleator method (Tandrup 1993) for cells counted in the disector probes. Cell counts and size measurements were made in four animals of either species. Coefficients of error for number estimates were calculated according to Gundersen et al. (1999) using the conservative $m = 0$ approach (Slomianka and West 2005). Statistical analysis were done using SPSS Statistics version 17.0.0 (SPSS Inc., Chicago, Illinois, USA). Cell sizes were compared by an ANOVA using cell type and species as fixed factors. Posthoc comparisons of cell sizes were made using LSD and Bonferroni tests, with a significance level of $P < 0.05$.

Image processing

Images of horizontal and coronal sections were captured at 5–40× magnification using a MBF CX9000 camera

(MicroBrightField Inc., Colchester, Vermont, USA). Adjustments were made to the brightness and colour of the images to restore their appearance in the microscope. No local changes were made unless noted in the figure legends. For three-dimensional modelling, EC fields were traced in Nissl-stained horizontal sections and assigned colours. Images were aligned using AutoAligner 6.0.0 (Bitplane AG, Zurich, Switzerland), and a three-dimensional representation was produced using Imaris 6.2.0 (Bitplane AG, Zurich, Switzerland).

Terminology

For the delineation of the EC, we initially consulted a Megachiroptera brain atlas (Baron et al. 1996a). Our description of the laminar structure follows Amaral et al. (1987), who used a composite of the descriptions provided by Ramón y Cajal (1988) and Lorente de Nó (1933). We have adopted Brodmann's cytoarchitectonic division of the EC into lateral entorhinal area (LEA; area 28a) and medial entorhinal area (MEA; area 28b) based on a distinction between layer II and layer III, which is clear in LEA but not in MEA (Brodmann 1909). The apparent size and position of the entorhinal fields, as they appeared in the three-dimensional reconstructions, matched best with the two-dimensional map provided by Amaral et al. (1987), and their nomenclature was adopted. We could, however, not consistently distinguish the E_{Lc} and E_{Lr} fields and treat them here collectively as E_L. In the bats, the E_L field lies in between fields E_I and E_R. Also, the E_O field, which appears as a small area rostral to E_R in primates, could not be consistently distinguished from the E_R field. MEA is comprised of caudal-limiting (E_{CL}) and caudal (E_C) entorhinal fields. LEA is constituted by two lateral fields, rostral (E_R), lateral (E_L), and a transitional area, the intermediate (E_I) entorhinal field.

One possible alternative to the primate nomenclature would have been that developed in rats (Insausti et al. 1997) and mice (van Groen 2001). However, most subfields identified based on histoarchitectural criteria in bats are very difficult to align topographically with those identified in rats and mice, which cast doubts on a possible homology of these fields. For example, the ME field is prominently ventral in location, in contrast to the E_C field in the bats which extends proportionally from dorsal to ventral. The lateral fields, DIE and DLE, extend rostrocaudally but in bats, as in primates, the corresponding fields, E_L and E_R, extend mediolaterally, obliquely to the rhinal sulcus. Although functional specialisations of the EC necessarily will result in differences in the detailed structure of subfields between species or larger phylogenetic groups, which have justified species-specific nomenclatures (e.g., guinea-pig: Uva et al. 2004; dog: Woźnicka et al. 2006), we do not believe that this is a productive approach in the long term for a cortical region that most likely shares basal functional aspects in all mammals.

Cellular morphological phenotypes were distinguished based on the earlier descriptions of Ramón y Cajal (1988), Germroth et al. (1991), Klink and Alonso (1997a) and Schwartz and Coleman (1981).

Results

Location and delineation of the entorhinal cortex

The location of the entorhinal cortex in the species investigated here corresponds to Brodmann's (1925) description of the area 28 in *Pteropus*, a related fruit bat species (Fig. 1a, b). Three-dimensional representations of the EC in Wahlberg's epauletted fruit bat and the straw-coloured fruit bat show the location and relationships of the fields (Fig. 1e–h). This corresponds to a caudo-ventral and lateral location of the EC in the piriform lobe (Fig. 1c, d). The rostral and lateral boundary of the EC is formed by the perirhinal and prepiriform cortex. Caudally and medially, it borders the para- and presubiculum. The ventro-medial boundary is delimited by part of the hippocampo-amygdaloid transition.

Medial entorhinal area (MEA)

Laminar structure Generally, layer I varies little. Layer II is not well delineated from layer III. A cell-sparse layer IV (lamina dissecans) is visible throughout the MEA, and layers V and VI are wide and densely populated (Fig. 2a, b).

Caudal-limiting entorhinal field (E_{CL})

This is the most caudal field of MEA, bordering the para- and presubiculum caudally and medially (Fig. 2a, b). It extends medio-laterally and briefly apposes the postrhinal cortex laterally (Fig. 1g, h).

Cytoarchitecture In both species, layer I is broad and has small light-staining neurons that are sparsely distributed. Layer II is well delineated from layer I and is densely populated in both species (Fig. 2c, d). Layer III is patchily populated by neurons of similar size. It is separated from layer V by a distinct, cell-sparse layer IV. Layer V is wide and has three sublayers. Sublayer Va is well developed and loosely populated by large intensely staining pyramidal neurons, and appears stratified in the straw-coloured fruit bat (Fig. 2a, c). Sublayer Vb has a dense population of small moderately staining cells (Fig. 2c, d). Sublayer Vc is

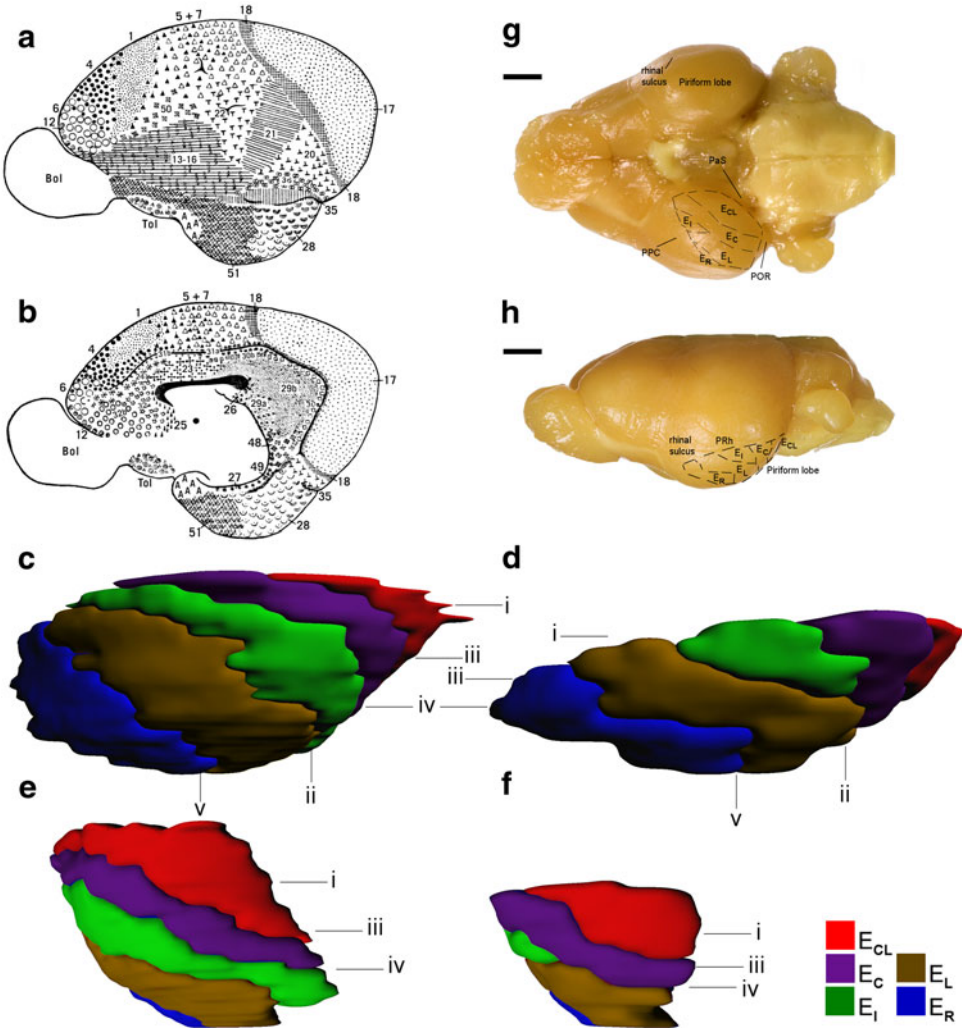

Fig. 1 Schematic drawing of the brain of Pteropus reproduced from Brodmann (1909). Lateral (**a**) and medial (**b**) views showing the location of Brodmann area 28. Three-dimensional representation of the entorhinal fields in the straw-coloured fruit bat (**c**, **e**) and Wahlberg's epauletted fruit bat (**d**, **f**) showing the approximate level of Figs. 2 and 3(*i*), 4(*ii*), 6(*iii*), 7, 8(*iv*) and 9(*v*). **c**, **d** Lateral view. **e**, **f** Caudal view showing the approximate level of Figs. 4(*iv*) and 9(*v*). Brain of Wahlberg's epauletted fruit bat showing a schematic drawing of the EC fields in the piriform lobe, and in relation to the perirhinal cortex (PRh), parasubiculum (PaS), postrhinal cortex (POR), prepiriform cortex (PPC) and rhinal sulcus. **g** Ventral view. **h** Lateral view. *Scale bars* 200 μm (**g**, **h**)

inconsistently visible as a narrow, cell-sparse zone separating layer V from layer VI. The three sublayers are more obvious in the straw-coloured fruit bat (Fig. 2a, c). Layer VI is wide and densely populated by small intensely staining neurons. Both layers V and VI are organised in radial columns. In both species, layer VI is not well demarcated from the white matter.

Chemoarchitecture Timm-staining of layer I of E_{CL} is pale superficially and dark innermost, dividing layer I into two parts, Ia and Ib (Fig. 3a, b). This pattern is recurrent in all medial and lateral entorhinal fields. Staining decreases from a dark layer II adjacent to layer I to a moderately stained deep layer III. This decrease is gradual in the straw-coloured fruit bat, whereas it appears more sudden, about half-way in layer III, in Wahlberg's epauletted fruit bat. Layer III is separated from layer V by a narrow light staining band corresponding to layer IV. Sublayer Va stains moderately in contrast to the lightly stained layers Vb and VI. There are no further apparent differences between the two species.

A sharp decrease in parvalbumin-like immunoreactivity marks the border of the caudal-limiting field towards the parasubiculum (Fig. 4c, d). Layer I has several processes oriented perpendicular to the cortical surface, which appear smooth or beaded (Fig. 5a). Layer II has few polygonal cell bodies with radial processes directed into layers I and III (Fig. 5a, b). The majority of cell bodies are located either proximally or distally in layer II. An intensely staining, dense fibre plexus extends in layers II and III (Fig. 5a). Layer III contains several cell bodies that are variable in size and shape (Fig. 5a, c–e). These include medium-sized to large polygonal cell bodies with vertically directed processes into layers II and IV, and spherical cell bodies with horizontal and ascending processes (Fig. 5c–e). Medium-sized to large polygonal cell bodies with radial processes that can be traced within the layer and into layer II are also observed (Fig. 5e). Most of these cell bodies are located in the lower half of layer III. More medial and caudal, immunoreactive cell bodies in layer III send processes into the parasubiculum (Fig. 5f). Staining

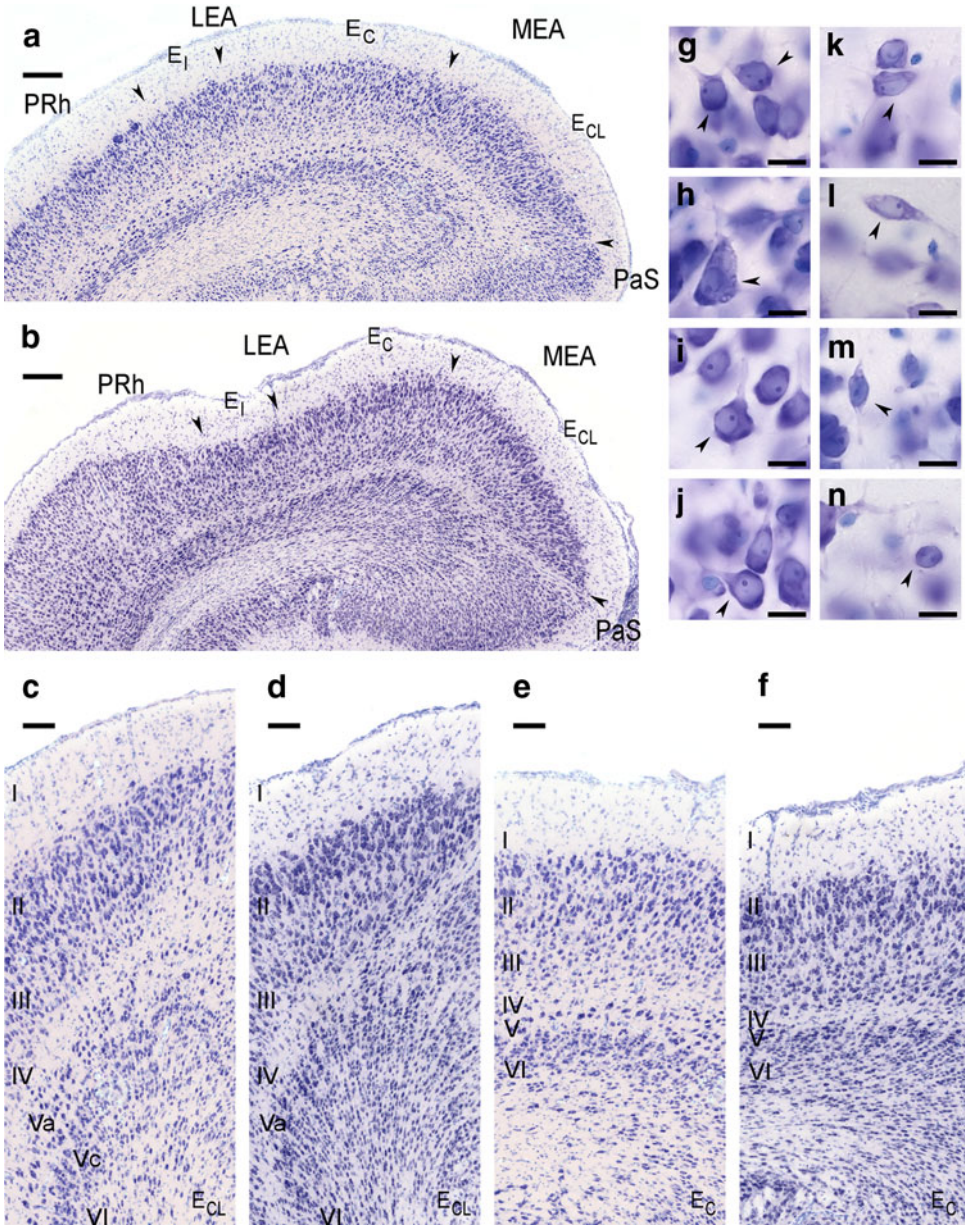

Fig. 2 Horizontal sections at a dorsal level showing rostrocaudal extent of fields E_{CL}, E_C, and E_I, indicated by *arrows* in the straw-coloured fruit bat (**a**, **c**, **e**, **g**) and Wahlberg's epauletted fruit bat (**b**, **d**, **f**, **h**). **c**, **d** E_{CL} layer II is well delineated from layer I; layer IV is prominent, and layers V and VI are radial and columnar. **e**, **f** E_C has an indistinct layer II and stratified Va in **e** and distinct layer II in **f**. Nissl-stained sections showing different neuronal phenotypes (indicated by *arrows*) in MEA layer II in Wahlberg's epauletted fruit bat (**g**, **i**–**m**) and the straw-coloured fruit bat (**h**, **m**). Pial surface is in the *top*. **g** Ovoid stellate cell, **h** polygonal stellate cell, **i** pyramidal cell, **j** oblique pyramidal cell, **k** horizontal tripolar cell, **l** bipolar cell, **m** fusiform cell, **n** small round cell. *Scale bar* **a**, **b** 300 μm; **c**–**f** 250 μm; **g**–**n** 50 μm

sharply drops at the border with layer IV (Fig. 5c). Layer IV has few small cell bodies with radiating processes and spindle-shaped cell bodies with short ascending and descending processes (Fig. 5g). Processes from cell bodies in the layers III and V cross through layer IV (Fig. 5c, h). Layer V has little reactivity. Large and medium-sized polygonal and conical cell bodies with processes directed into layers III, VI and white matter are observed (Fig. 5i, j). A sparse fibre plexus is observed in layers V and VI (Fig. 5h, j, k). Cells are rare in layer VI (Fig. 5k). There are no apparent species differences.

In Wahlberg's epauletted fruit bat, a SMI-32-like immunoreactive fibre plexus and few cell bodies are present in layers II and III (Fig. 4f). SMI-32-like immunoreactivity is not observed in the EC of the straw-coloured fruit bat (Fig. 4e), while characteristic SMI 32-like staining of neocortical neurons is present in this species (Fig. 5n).

Caudal entorhinal field (E_C)

This is the central field of the MEA, located lateral to field E_{CL} and adjacent to the LEA (Fig. 2a, b). Dorso-laterally it apposes the perirhinal cortex and parasubiculum ventromedially (Fig. 1g, h).

Cytoarchitecture Layer I is broad and well delineated from the layer II. Layer II is wide, moderately cell-dense, and

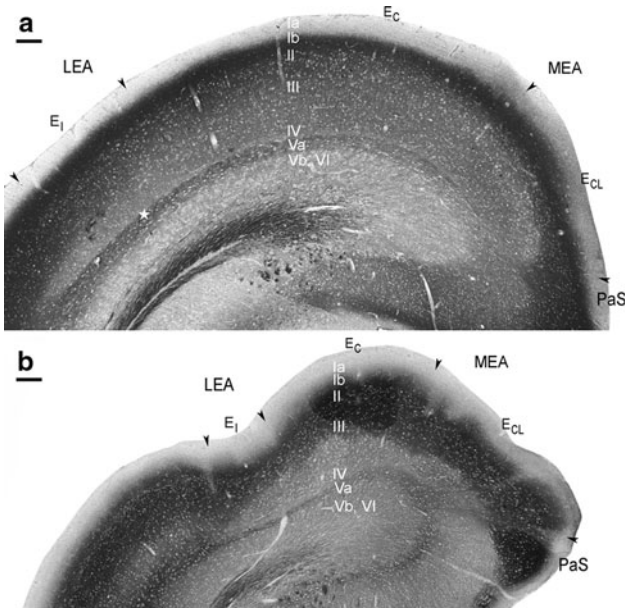

Fig. 3 Timm-stained horizontal sections showing the rostrocaudal extent of E_{CL} and E_C. Deep layer I and II stain darkly, layer III is moderately staining and is separated from a dark sublayer Va by a narrow pale layer IV. Deeper layers are pale staining. **a** Straw-coloured fruit bat. A staining artefact was removed (indicated by *star*). **b** Wahlberg's epauletted fruit bat. *Scale bar* 300 μm

some layer II cells scatter into the deep part of layer I. It is less cell-dense compared to layer II in E_{CL}. Similar to E_{CL}, cells are homogeneously distributed within the layer (Fig. 2a, b, e, f). In the straw-coloured fruit bat (Fig. 2e), and Wahlberg's epauletted fruit bat (Fig. 2f), layer II is populated by varied neuronal phenotypes. Cell-sparse zones between layers II and III are infrequent. Layer III pyramidal neurons are homogenously sized and organised in columns. Layer IV is prominent although narrower in comparison to E_{CL}. Layer V is wide and sublayers Va and Vb are visible; Va is loosely populated and has the stratified appearance observed in field E_{CL} in the straw-coloured fruit bat (Fig. 2e), and Vb is closely apposed to layer VI. Layers V and VI of E_C are not only narrow in comparison to E_{CL} but are also organised in a radial columnar pattern. In both species, layer VI is not sharply demarcated from the white matter.

Chemoarchitecture The Timm-staining of E_C shows similarity in pattern and intensity to field E_{CL} (Fig. 3a, b). Parvalbumin-like immunoreactivity decreases in comparison to E_{CL}, but the staining pattern is the same (Fig. 4c, d). Layer I has immunoreactive processes, and the fibre plexus in layers II and III stains intensely. Cell bodies are observed in layers II to VI.

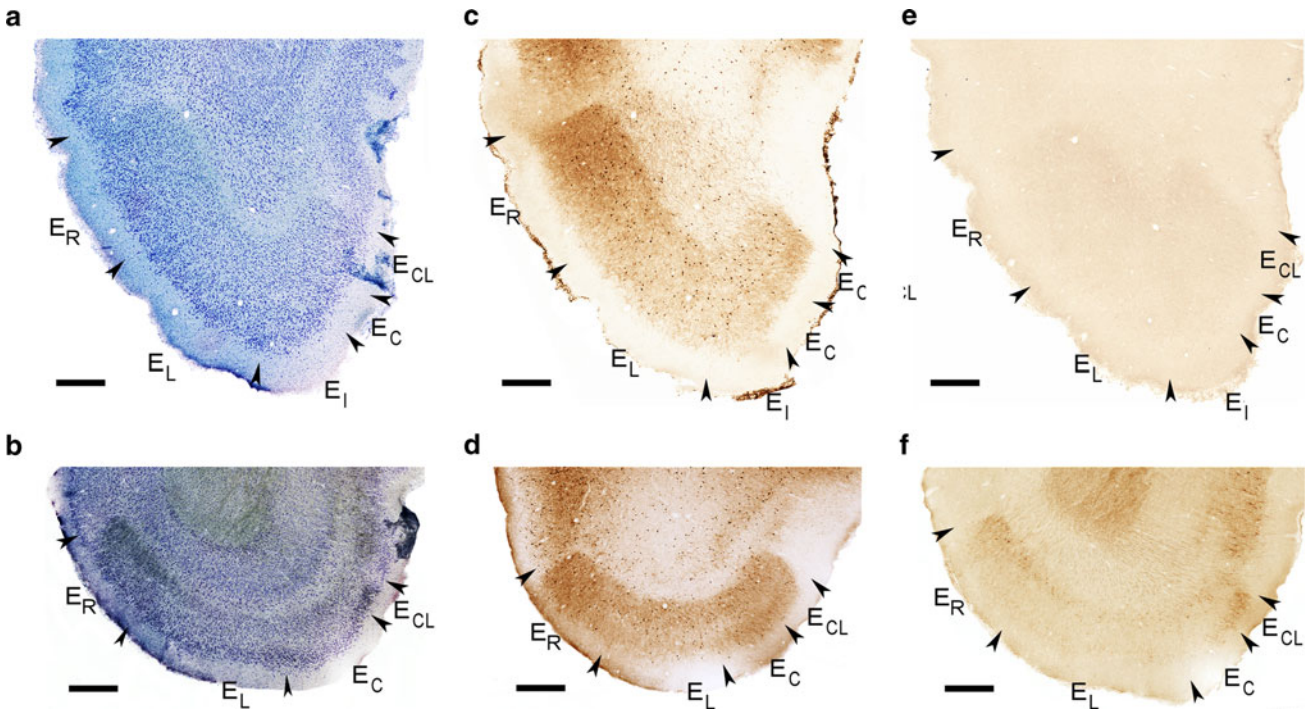

Fig. 4 Coronal sections at a caudal level showing the mediolateral extent of the fields, indicated by *arrows*, in the straw-coloured fruit bat (**a**, **c**, **e**) and Wahlberg's epauletted fruit bat (**b**, **d**, **f**). **a**, **b** Nissl-stained. **c**, **d** Parvalbumin-like reactivity of neurons and fibre plexus involving layers II and III. Most reactivity is observed in E_{CL}, E_L and E_R. **e** Lack of SMI 32-like staining in the straw-coloured fruit bat. **f** SMI 32-like staining in layers II and III of E_{CL}, E_L and E_R of Wahlberg's epauletted fruit bat. *Scale bar* 300 μm

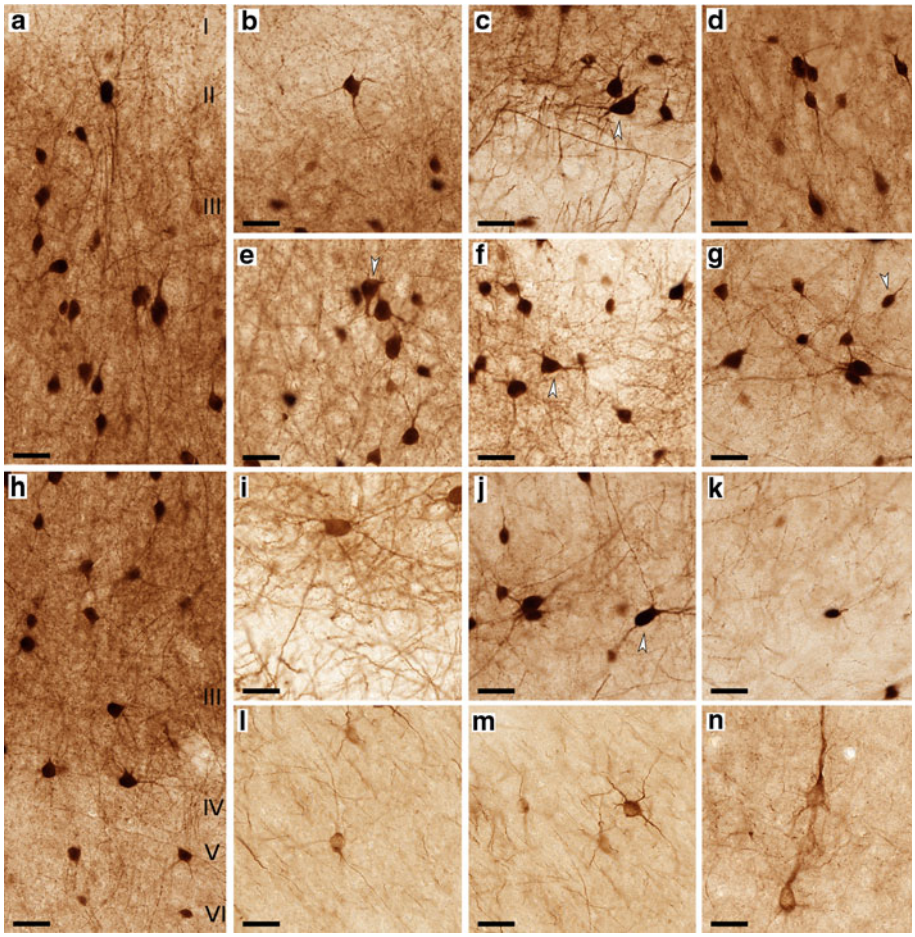

Fig. 5 Parvalbumin-like stained sections in Wahlberg's epauletted fruit bat (**a**–**h**, **j**, **k**) and the straw-coloured fruit bat (**i**). **a** Fibre plexus and several neurons and processes in layers I–III. **b** Multipolar neuron in layer II with processes that extend into layer I. **c** Layer III is well delineated from the weakly stained layer IV. Large spherical multipolar neuron with an ascending thick and descending thin processes, next to a horizontally oriented neuron (*arrow*). **d** Medium-sized conical neurons with thick ascending processes in mid layer III. **e** Large inverted multipolar neuron (*arrow*) with a thick descending process next to a spherical multipolar neuron in layer III. **f** Large multipolar neuron (*arrow*) in layer III sends a process into the weakly stained border between E_{CL} and parasubiculum. **g** Unipolar neuron (*arrow*) in layer IV and few spherical neurons in layers V. **h** Survey of layers II–VI. **i** Multipolar neuron in layer V with radial processes. **j** Large conical neuron (*arrow*) with long smooth ascending and descending processes in layer V. **k** Small unipolar cell in layer VI. SMI 32-like staining in Wahlberg's epauletted fruit bat (**l**, **m**). **l** Pyramidal neuron in layer III. **m** Multipolar neuron in layer III. **n** SMI 32-like stained pyramidal neurons in the somatosensory cortex in the straw-coloured fruit bat. *Scale bar* 100 μm

SMI-32-like staining is weak in Wahlberg's epauletted fruit bat (Fig. 4f), and absent in the straw-coloured fruit bat (Fig. 4e).

Lateral entorhinal area (LEA)

The LEA approximates the perirhinal cortex rostrally and dorsally, the prepiriform cortex ventrolaterally, and the hippocampo-amygdaloid transition area ventromedially.

Laminar structure Within the three fields of the LEA, variations in cellular density and arrangement across the layers are observed (Figs. 6a, b, 7a, b). Neurons in layer II group together in patches and clusters. A narrow cell-free zone is visible between layers II and III, especially in more lateral and rostral fields. Layer IV is generally narrow and visible mainly in field E_I, adjacent to the MEA. Layers V and VI are narrower and organised in rows. Sublayer Va is wide in most of this subdivision. Layers Vb and VI in the LEA are narrow and closely apposed in comparison to those in the MEA.

Intermediate entorhinal field (E_I)

This field is the most caudal and medially located of the LEA (Fig. 6a, b). It is dorso-medial to rhinal sulcus, and it first apposes the perirhinal cortex dorso-medially and subsequently field E_L (Fig. 1g, h). Characteristics of both the MEA and LEA are observed in the laminar organisation of E_I; the superficial layers share characteristics with the LEA,

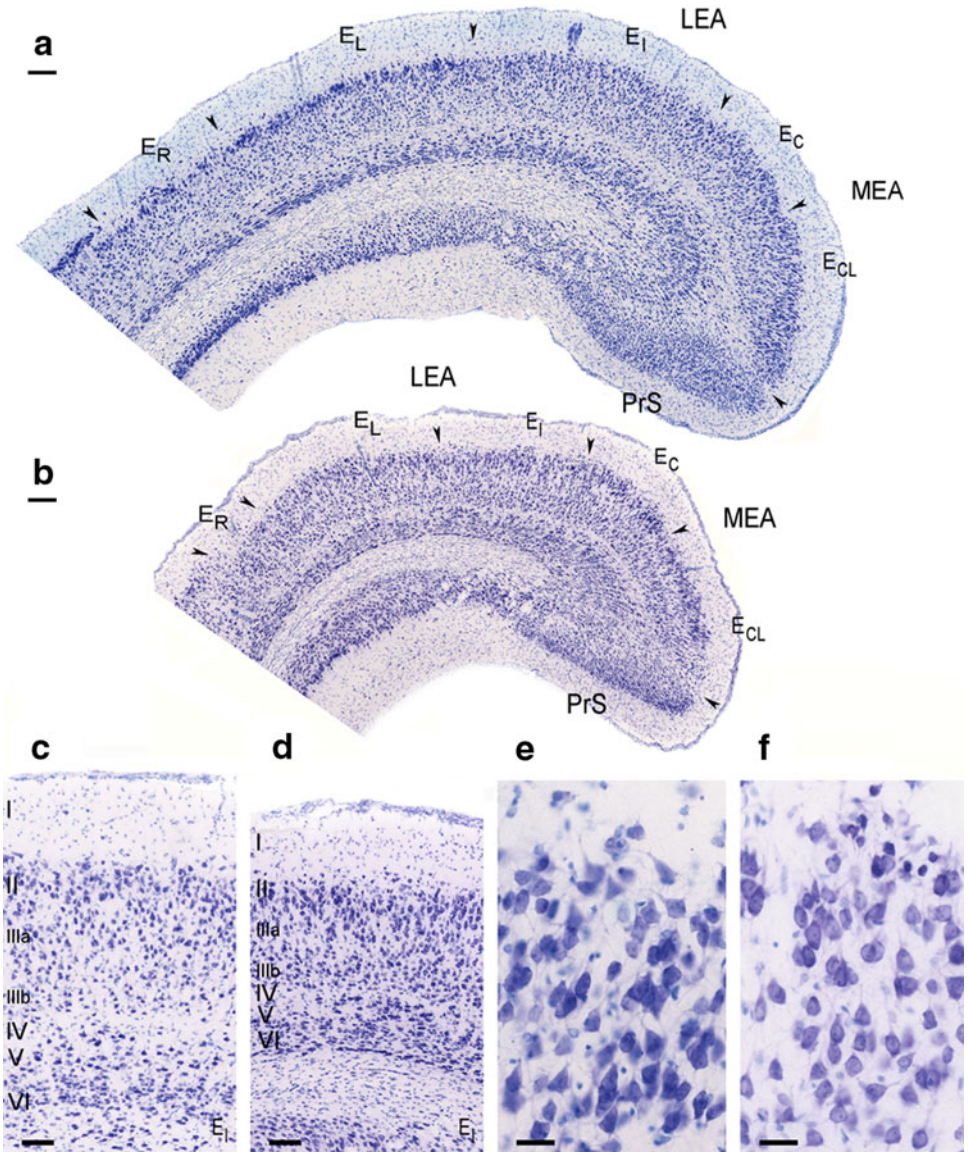

Fig. 6 Horizontal sections at mid dorsoventral level showing the extent of fields E_I, E_L and E_R, indicated by *arrows*, in the straw-coloured fruit bat (**a**, **c**, **e**) and Wahlberg's epauletted fruit bat (**b**, **d**, **f**). **c**, **d** E_I field has a layer II with dispersed neurons, and deep layers have a radial columnar organisation. Layer VI is not well delineated from the white matter in **c**. **e** Small dark staining neurons in layer II. **f** Multiple neuronal phenotypes in layer II. *Scale bar* **a**, **b** 300 μm; **c**, **d** 250 μm; **e**, **f** 100 μm

while the deep layers show characteristics more consistent with MEA. This field could therefore be termed a transition area. It extends to the ventral pole of the EC in the straw-coloured fruit bat (Fig. 1c, e), apposing the parasubiculum ventro-medially and the hippocampal-amygdaloid transition area ventro-rostrally. It is only found in the dorsal one-half of the EC in Wahlberg's epauletted fruit bat (Fig. 1d, f).

Cytoarchitecture Layer I is broad and has lightly stained sparsely distributed small neurons. Layer II is wide (Fig. 6a, b). Neurons disperse from layer II into layer I and some of them appear as ectopic neurons in layer I (Fig. 6c–f). Small dark staining cells are noted in Wahlberg's epauletted fruit bat (Fig. 6f). Occasionally narrow cell-sparse zones are found within layer II and between layers II and III. Neurons in layer III are more evenly distributed than in field E_C, and superficially (sublayer IIIa) neurons are larger than those deeper in the layer (Fig. 6c, d). Layer IV is prominent in both species. Sublayer Va in E_I is comparable in width to E_C. The large pyramids are stratified within the layer in the straw-coloured fruit bat (Fig. 6a, c), but appear closely associated with sublayer Vb in Wahlberg's epauletted fruit bat (Fig. 6b, d). Deeper, layer V is confluent with layer VI, and these layers are narrower compared to those in E_C, but retain the radial columnar organisation (Fig. 6c, d). Layer VI gradually merges with the white matter in the straw-coloured fruit bat (Fig. 6a, c).

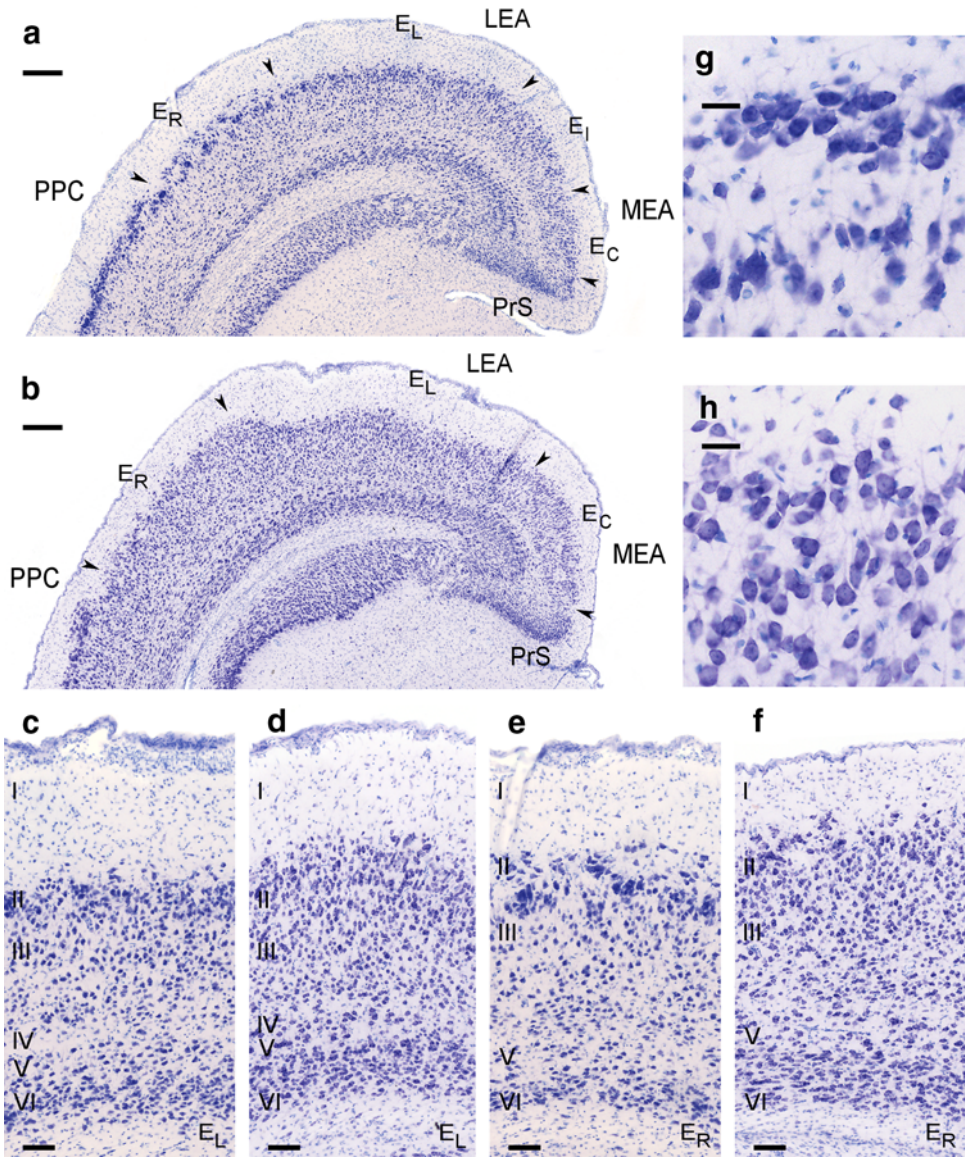

Fig. 7 Horizontal sections at a ventral level showing extent of the lateral fields, E_I, E_L and E_R, indicated by *arrows*, in the straw-coloured fruit bat (**a**, **c**, **e**, **g**) and Wahlberg's epauletted fruit bat (**b**, **d**, **f**, **h**). **c**, **d** E_L has a layer II with clustered neurons better visible in **c**, patchy layer III and wide Va. **e**, **f** E_R has clustered layer II neurons, more distinct in **e**. **g**, **h** Layer II clusters. *Scale bar* **a**, **b** 300 μm; **c**–**f** 250 μm; **g**, **h** 100 μm

Chemoarchitecture In both species, Timm-staining pattern and intensity in E_I are similar to that of the E_{CL} and E_C fields (Figs. 3a, b, 8a, b). A pale layer IV is occasionally observed (Fig. 8b). A moderately stained layer V is present (Fig. 8a, b). Parvalbumin-like staining is faint, comprising a loose fibre plexus, few cell bodies and processes in layers II–V (Fig. 9c, d). SMI-32-like staining is weak in Wahlberg's epauletted fruit bat (Fig. 9f) and absent in the straw-coloured fruit bat (Fig. 9e).

Lateral entorhinal field (E_L)

This field is rostral to E_I. It apposes the perirhinal cortex dorso-laterally, and is caudal to E_R ventrally (Fig. 7a, b). Ventro-medially it apposes the presubiculum and subsequently the hippocampal-amygdaloid transition area.

Cytoarchitecture Layer I is broad, and ectopic layer II neurons are common (Fig. 7c, d). Layer II in the straw-coloured fruit bat has dense cell clusters that are separated by areas of low cell density (Figs. 6a, 7a). Although there are cell dense areas within layer II of Wahlberg's epauletted fruit bat, variations in cell density are much less pronounced than in the straw-coloured fruit bat (Figs. 6b, 7b). A narrow cell-sparse zone is infrequently visible between layers II and III. In both species, layer III is wide and moderately populated. In the straw-coloured fruit bat, neurons are more dispersed than in field E_I (Fig. 7a). In both species, superficially (sublayer IIIa), neurons are densely distributed and appear larger compared to those deeper in the layer (Fig. 7c, d). Layer IV is sometimes present. Layer Va is wider and more populated than in E_I in both species (Figs. 6a, b, 7a, b). Sublayer Vb and layer VI

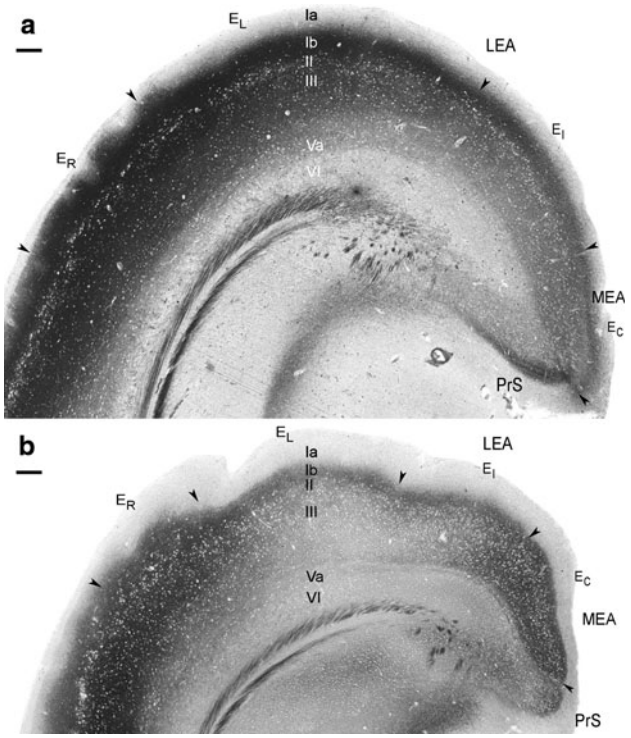

Fig. 8 Timm-stained horizontal sections at a ventral level showing the rostrocaudal extent of fields E_I, E_L and E_R, indicated by *arrows*. Deep layers I, II and III stain darkly, Va stains moderately and Vb and layer VI are pale staining. **a** Straw-coloured fruit bat. **b** Wahlberg's epauletted fruit bat. *Scale bar* 300 μm

are closely apposed, but, in contrast to E_I, they do not appear laminated (Fig. 7c, d). Layers Vb and VI are narrower in comparison to those in E_I, which is more marked in the straw-coloured fruit bat (Fig. 7a).

Chemoarchitecture A strong Timm reaction is noted in the E_L field in the straw-coloured fruit bat (Fig. 8a) and less so in Wahlberg's epauletted fruit bat (Fig. 8b). A pale sublayer Ia contrasts with a darkly stained sublayer Ib. Layers II and III stain moderately in Wahlberg's epauletted fruit bat and darkly in the straw-coloured fruit bat. A moderately stained layer Va is observed. Layers Vb and VI are lightly stained. In both species, parvalbumin-like immunoreactive processes and cell bodies stain with moderate intensity (Figs. 4c, d, 9c, d). In Wahlberg's epauletted fruit bat, SMI 32-like weakly stained cell bodies and processes in layer III are noted (Fig. 4f). No staining is observed in the straw-coloured fruit bat (Figs. 4e, 9e).

Rostral entorhinal field (E_R)

Rostrally, this lateral field is located close to a very shallow rhinal sulcus, dorso-laterally adjoining the perirhinal (Figs. 1h, 6a, b) and prepiriform cortex ventrolaterally (Figs. 1g, 7a, b).

Cytoarchitecture In both species, layer I narrows and layer II is characterised by a decrease in cell density in comparison to other fields (Figs. 6a, b, 7a, b). Layer II has two sublayers separated by cell-sparse zones. This is more distinct in the straw-coloured fruit bat (Figs. 6a, 7a), where superficially sublayer IIa neurons forms narrow and discontinuous bands (Fig. 7e, g). Sublayer IIb is wider than IIa. Cell clusters and areas of lower cell density alternate in a manner similar to layer II in E_L (Fig. 7a, e). Frequent narrow cell-sparse zones extend through layer II into layer III (Fig. 7e). In Wahlberg's epauletted fruit bat, IIa neurons are few, scattered and tend to be located close to IIb (Figs. 6b, 7b). Sublayer IIb is more cell-dense (Fig. 7f, h) than in the straw-coloured fruit bat, and cell clusters are not observed (Fig. 7b, f). Layer II narrows and appears to merge with layer III at the junction of the EC with the perirhinal (Fig. 6a, b) and prepiriform cortex (Fig. 7a, b). Elsewhere, layer II is separated from layer III by cell-sparse zones. Layer III is wide and patchily organised superficially, less noticeably in Wahlberg's epauletted fruit bat (Fig. 7e, f). Deeper, layer III has a population of smaller pyramidal neurons. Layer IV is infrequently observed in Wahlberg's epauletted fruit bat and cannot be distinguished in the straw-coloured fruit bat. Sublayer Va is wider and more populated in comparison to field E_L (Fig. 7a, b). The large pyramidal neurons are stratified within the layer in the straw-coloured fruit bat (Fig. 7a, e), but this organisation is less obvious in Wahlberg's epauletted fruit bat (Fig. 7b, f). Layers Vb and VI have the same width as those in E_L in Wahlberg's epauletted fruit bat (Fig. 7b), but these layers thin along the rostral–lateral extent in the straw-coloured fruit bat (Fig. 7a). A columnar organisation of layers Vb and VI is observed in the straw-coloured fruit bat (Fig. 7a, e).

Chemoarchitecture Field E_R shows a pale layer Ia, dark Ib, II and III, moderately staining Va and pale Vb and VI (Fig. 8a, b). The Timm-staining pattern and intensity is similar to that of field E_L in the straw-coloured fruit bat (Fig. 8a). Darkly stained protuberances are observed in sublayer Ia, giving a wavy appearance (Fig. 8a, b). Parvalbumin-like immunoreactivity in E_R is strong (Fig. 9c, d) with a pattern that is similar to that of E_{CL} (Fig. 4c, d). The fibre plexus is intensely stained, as are the cell bodies and processes in layers II to V. Layer VI is weakly reactive. Parvalbumin-like reactivity decreases at the border between E_R and perirhinal (Fig. 9c, d) and prepiriform cortex (Fig. 4c, d). In Wahlberg's epauletted fruit bat, SMI 32-like staining is observed between layers II and VI (Figs. 4f, 9f). Fine and sometimes thick, vertically oriented processes run between the layers and cross the white matter. Layer II has few cell bodies. A band of conical and polygonal cell bodies is seen in the

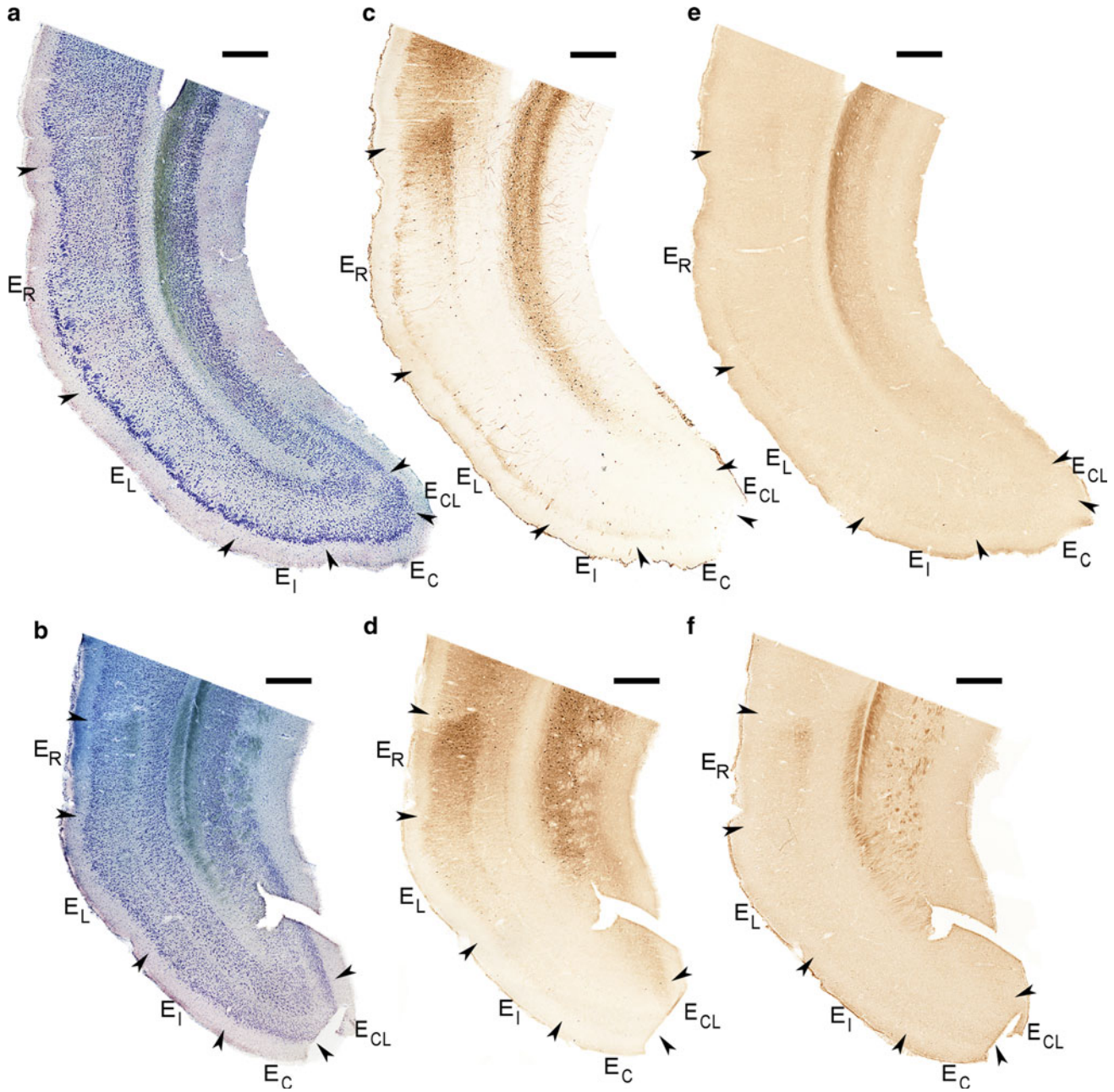

Fig. 9 Coronal sections at a rostral level showing the mediolateral extent of the fields, indicated by *arrows*, in the straw-coloured fruit bat (**a**, **c**, **e**) and Wahlberg's epauletted fruit bat (**b**, **d**, **f**). **a**, **b** Nissl-stained. **c**, **d** Parvalbumin-like reactivity of neurons and fibre plexus in field E_R. **e** Lack of SMI 32-like staining. **f** SMI 32-like staining in layer III in field E_R. *Scale bar* 300 μm

deep part of layer III (Figs. 4f, 5l, m). Some of these cell bodies are small, stain lightly and have apical and basal processes that can be traced for a short distance within the layer. Other cell bodies are larger, stain intensely, and their radiating processes can be traced in adjacent layers (Fig. 5l, m). Layer V has rare large cell bodies. The intensity of staining increases rostrally in this field.

Cell numbers and phenotypes in MEA layer II

Morphological phenotypes Ovoid stellate cells are spherical and oriented vertically (Fig. 2g). Large, trapezoid stellate cells that are either transversely or vertically oriented are referred to as polygonal stellate (Fig. 2h). Pyramidal cells are medium-sized to large, conical bodies with a large apical process oriented perpendicular to the pial

Table 1 MEA layer II neuronal phenotypes, profile areas and proportions

Cell type	Species	*N*	Mean area (μm^2)	SD (μm^2)	Proportion (%)
Ovoid stellate	*E. helvum*	352	162	44	35.8
	E. wahlbergi	193	164	46	40.8
Polygonal stellate	*E. helvum*	48	193	51	4.9
	E. wahlbergi	61	212	60	12.9
Pyramidal	*E. helvum*	181	196	51	18.4
	E. wahlbergi	83	232	61	17.5
Oblique pyramidal	*E. helvum*	62	192	43	6.3
	E. wahlbergi	23	212	66	4.9
Other	*E. helvum*	339	115	39	34.5
	E. wahlbergi	113	98	26	23.9
All cells measured	*E. helvum*	982	156	54	100
	E. wahlbergi	473	168	67	100

Table 2 Total number of neurons in MEA layer II

Species	Animal	Estimated total cell number	CE
E. helvum	1	56,067	0.06
	2	61,632	0.08
	3	56,265	0.09
	4	74,123	0.08
E. wahlbergi	1	31,712	0.09
	2	27,344	0.1
	3	33,147	0.08
	4	30,497	0.1

surface (Fig. 2i). Oblique pyramidal cells resemble the pyramidal cells, but have an apical process that is directed obliquely to the pial surface (Fig. 2j). 'Other' cells include generally small cells of tripolar (Fig. 2k), round (Fig. 2l), bipolar (Fig. 2m), or fusiform (Fig. 2n) appearance and medium-sized multipolar neurons. Cells of this class are located mostly superficially in layer II.

Sectional areas of neuronal phenotypes and the contribution of these phenotypes to the layer II cell population are listed in Table 1. Significant main effects were found for species, cell type and species × cell type interactions ($P < 0.001$ for all comparisons), with Wahlberg's epauletted fruit bat having a larger mean cell area for the polygonal stellate and pyramidal cell types, while 'other cells' are smaller in this species. In the comparison of cell sizes, stringent Bonferroni and lenient LSD posthoc testing produced identical outcomes in terms of significant differences between phenotypes. Ovoid stellate cells are different in size from all other cell types ($p_{LSD} < 0.001$ for all comparisons); polygonal stellate, oblique pyramidal and pyramidal cells are similar in size (polygonal stellate vs. pyramidal: $p_{LSD} = 0.46$, polygonal stellate vs. oblique pyramidal: $p_{LSD} = 0.37$, pyramidal vs. oblique pyramidal: $p_{LSD} = 0.09$) but different from other cell types ($p_{LSD} < 0.001$ for all other comparisons).

Layer II in the straw-coloured fruit bat has an estimated mean total cell count (Table 2) of 62,022 (SD 8,469, CE = 0.08), and in Wahlberg's epauletted fruit bat 30,675 (SD 2,470, CE = 0.09).

Discussion

We have provided a detailed description of the laminar and areal organisation of the megachiropteran entorhinal cortex using markers that have helped to define these regions in other species as well. In the following, the differences between the two bat species, rodents and primates, summarised in Table 3, are discussed from an anatomical and functional perspective.

Cytoarchitectonic comparison

Medial entorhinal area (*MEA*) Layer II of the most caudal and medial field is broad, continuous and well delineated from layer I above in the bats, primates and rodents. The islands described in the adjacent field, E_C (primates) (Amaral et al. 1987), are not well developed in the bats and rodents (Insausti et al. 1997). Layer III is similarly organised in the bats, primates and rodents, starting off patchy caudally, but progressively adopting a columnar arrangement in E_C and in the less caudal MEA field (ME) in rodents. Differences in cellular density in IIIa and IIIb are described in ME, but this is neither observed in the bats nor described in the primates. Layer IV is well developed in the bats and rodents but poorly visible or absent in the primates. Layer V in the bats, primates and rodents is well developed, with sublayers Va and Vb. The

Table 3 Summary of cytoarchitectural comparison between bats, primates and rodents

Region	Comparison
E_{CL}/CE	Layers II and III mostly similar
	Poorly developed layer IV in primates
	Layer Va moderately developed in rodents, well developed in bats and best developed in primates
E_C/ME	Layer II well differentiated in rodents and Wahlberg's epauletted fruit bat but islands only in primates
	Layer III bilaminar only in rodents
	Deep layers as in the E_{CL}/CE
E_I/VIE	Layer II moderately differentiated in bats and rodents, distinct islands only in primates
	Well developed layers III and IV in rodents, primates and bats
	Well-defined Va only in primates and bats
E_L/DLE	Layer II well differentiated in the straw-coloured fruit bat and rodents but distinct islands only in primates, poorly differentiated layer II in Wahlberg's epauletted fruit bat
	Wide layer III in bats and primates, narrow in rodents
	Layer IV absent in primates
	Layer Va well developed in primates and bats, indistinct Va in rodents
E_R/DIE	Indistinct islands in layer II of the straw-coloured fruit bat and rodents, wide cell islands in primates
	Bilaminar wide layer III in bats, rodents and primates
	Layer IV well developed in mouse, poorly developed in Wahlberg's epauletted fruit bat and rat, absent in straw-coloured fruit bat and primates
	Layer Va poorly developed in rodents, well developed in bats, all sublayers best developed in primates
	Well-developed layer VI in mouse, primates, and Wahlberg's epauletted fruit bat

CE, ME, VIE, DIE, DLE refer to regions in rodents

pyramidal cells of Va appear as 1–2 bands in Wahlberg's epauletted fruit bat, and appear closely apposed to Vb, which is also observed in rodents. Sublayer Va in the straw-coloured fruit bat is as well developed as in primates, showing 3–4 bands of pyramids. Sublayer Vc, which is prominent in the medial fields in primates, is infrequently visible in the bats and not described in rodents (Amaral et al. 1987; Blaizot et al. 2004; Insausti et al. 1997; van Groen 2001).

Lateral entorhinal area (*LEA*) Of the lateral fields, E_I shows similarity between the two bat species. The intermediate field is referred to as VIE in the rodents (Insausti et al. 1997). Similar characteristics found in rodents, primates and bats include layer II clusters and a patchy layer III. Layer II islands are a feature in the primates that is absent in both bats and rodents. The bilaminar layer III, presence of layer IV and a well-defined Va are characteristics shared by the bats and primates in E_I but not rodents (Amaral et al. 1987; Insausti et al. 1997; van Groen 2001).

Clustering in layer II is observed in E_L field in the straw-coloured fruit bat, primates and the corresponding DLE in rodents (Amaral et al. 1987; Insausti et al. 1997; van Groen 2001). If clustering is a distinctive feature of this subdivision, then Wahlberg's epauletted fruit bat has a poorly differentiated layer II. Cell-sparse zones infrequently separate layers II and III in the rodents and bats but only in a caudal part of the LEA in primates. Layer III has a bilaminar character, observed in rodents and bats, but not in primates. While layer III is narrow in the rodents, it is wide in the bats and primates. Layer IV is infrequently visible in the bats and rodents and absent in the primates. Layer Va is prominent in the bats and primates (Amaral et al. 1987). Layer V in rodents is narrow and comprised mostly of sublayer Vb, and few pyramids in Va (Insausti et al. 1997; van Groen et al. 2003). Layer VI has a less-stratified appearance in bats, primates and rodents.

The layer II clusters in E_R field are separated by cell-sparse zones into indistinct islands in the straw-coloured fruit bat, but they do not develop into the wide cell islands distinctive of primate LEA layer II (Amaral et al. 1987; Blaizot et al. 2004). The corresponding field in rodents, DIE (Insausti et al. 1997; van Groen 2001) appears similar to the straw-coloured fruit bat. Cell-sparse zones separating layers II and III in the E_R field described in the primates

and rodents are observed in the bats, less frequently in Wahlberg's epauletted fruit bat. The wide and bilaminar character of layer III in the bats is consistent with descriptions made in related fields in primates and rodents. In the straw-coloured fruit bat and primates, layer IV is not visible in the E_R field (Amaral et al. 1987). Similar observations have been made in a corresponding field, Pr2 in the rhesus monkey (van Hoesen and Pandya 1975). Layer IV is present in the mouse (van Groen 2001) and infrequently observed in Wahlberg's epauletted fruit bat and the rat (Insausti et al. 1997). Layer Va is wide and has 3–4 rows of pyramids, more so in the straw-coloured fruit bat, resonating with descriptions made in primates (Amaral et al. 1987; Blaizot et al. 2004). The pyramids associated with this layer appear incidentally in rodents (Insausti et al. 1997; Mulders et al. 1997). All three sublayers of layer V are only consistently observed in primates. Layers Vb and VI narrow rostrally in the straw-coloured fruit bat. In the rat, only layer VI narrows (Insausti et al. 1997). In Wahlberg's epauletted fruit bat, mouse (van Groen et al. 2003) and primates (Amaral et al. 1987), layer VI is well developed.

Chemoarchitectonic comparison

Timm-staining reveals the laminar organisation of the EC, which assisted in delineating the EC from adjacent structures, and distinguished between medial and lateral subdivisions and their layers. In the two species, dark staining is observed in layers Ib and II in all fields and part of layer III in the E_R field. Layer Va stains moderately, and layers IV, Vb and VI are pale. The staining pattern corresponds to the presence of zinc in the boutons of the terminals of telencephalic afferents to the EC (Perez-Clausell and Danscher 1985; Slomianka 1992), where zinc may serve as a neuromodulator of excitatory transmission (Frederickson et al. 2005; Paoletti et al. 2009). The distribution of zinc-containing boutons in bats is comparable to observations made in the guinea pig, dog and pig (Geneser-Jensen et al. 1974; Holm and Geneser 1989; Wóznicka et al. 2006). In the rat and mouse, the staining is moderate in layers Ib and II of MEA and increases gradually across layer III to become very intense at the layer III/IV boundary (Slomianka 1992; Slomianka and Geneser 1991).

Parvalbumin-like immunostaining varies along a mediolateral gradient, and is comparable in the two fruit bats. Staining mainly occurs in the E_R, E_L and medial fields, and an intermediate reactivity in the E_I field. Parvalbumin is present in GABAergic interneurons of the EC in layers II, III, V and VI and predominantly expressed by chandelier and basket cells (DeFelipe et al. 1989; Fonseca et al. 1993; Hendry et al. 1989). Observations in the fruit bats are consistent with reported distributions of parvalbumin in rat (Wouterlood et al. 1995), guinea pig (Uva et al. 2004), macaque (Pitkänen and Amaral 1993) and human EC (Beall and Lewis 1992; Tuñón et al. 1992). Thus, there does not seem to be much difference in the role of this calcium-binding protein and the part of the inhibitory circuitry identified by it in the EC across species (Hof and Sherwood 2005).

SMI-32 recognises a high molecular weight (200kD) non-phosphorylated neurofilament protein H (Sternberger and Sternberger 1983) in neuronal soma, dendrites and some large calibre axons of specific subpopulations of neurons resulting in a distinct cellular and laminar staining pattern. This protein also occurs in a subset of cortical neurons selectively lost in Alzheimer's disease (Hof et al. 1990; Morrison et al. 1987). In Wahlberg's epauletted fruit bat, immunoreactivity in particular defines layer III of the EC. Most of the staining is observed in the E_R and medial fields. Rostrally, the staining in layers II, III and V concurs with observations made in the E_L field of the macaque and human, where a rostral–caudal gradient was noted (Beall and Lewis 1992; Saleem et al. 2007). The prevalent staining of layer III is in contrast to the macaque, where it mainly involves layers II and V of LEA (Saleem et al. 2007). A comparative analysis in the visual cortex shows similarities in regional staining patterns between closely related species; these patterns are shown to be predictive of evolutionary relationships (Hof et al. 2000). This may imply that the two bat species may not be as phylogenetically close as we presume. It could also be that the EC is a less adept model for this hypothesis, and a lack of immunoreactivity in the EC of the straw-coloured fruit bat may indicate that the function subserved by SMI-32 immunoreactive cytoskeletal components may either not be required or is assumed by another protein (Campbell and Morrison 1989; Goldstein et al. 1983). There are similar reports of a lack of SMI-32 immunoreactivity in the EC that include an Australian echidna (*Tachyglossus aculeatus*) and the Tamar wallaby (*Macropus eugenii*) (Ashwell et al. 2005; Hassiotis et al. 2004, 2005).

Cytoarchitectural synopsis

Overall, the organisation of the EC cannot be categorised as either primate- or rodent-like; rather the EC shows a mosaic of characters. The two bat species share, e.g., a well-developed layer Va throughout the EC with primates, while they share with rodents the absence of distinct layer II islands in most EC fields. Species-specific characteristics are largely restricted to layer II, which is better differentiated in the MEA of Wahlberg's epauletted fruit bat, while it, in comparison to the straw-coloured fruit bat, is poorly differentiated in the LEA. Buhl and Dann (1991) already noted a primate-like dispersion of hippocampal pyramidal

Table 4 Indices for encephalisation (EI), neocorticalization (NEO) and the sizes of the hippocampus (HIP) and schizocortex (SCH) for the bats investigated in this study, rat and the major primate groups

Species	EI	NEO	HIP	SCH
E. helvum[a]	311	1,088	283	373
E. wahlbergi[a]	302			
E. labiatus[a]	292	999	281	328
Rattus norwegicus[b]	155	475	132	122
Prosimian primates[c]	415	2,100	~290	~360
Simian primates[c]	801	5,100	~280	~320
Human[c]	3,012	20,000	~500	~680

For *E. wahlbergi* only the encephalisation index is available. *Epomophorus labiatus*, which is equal in body weight to *E. wahlbergi*, was included to present values for NEO, HIP and SCH

[a] Data from Baron et al. (1996b)

[b] Calculated from Baron et al. (1996b) and Kruska (1975)

[c] Calculated from Stephan et al. (1986)

cells, which we also observed in the species investigated here, and which in other species provide hippocampal afferents to the EC layer Va (Swanson and Cowan 1977). The EC layer Va, in turn, provides afferents to neocortical areas (Swanson and Köhler 1986).

Fruit bats share with primates high indices for encephalization and neocorticalization as well as high indices for the size of the schizocortex (Table 4). The schizocortex contains, in addition to the entorhinal cortex, the pre- and parasubiculum as well as the perirhinal cortex. While an interference from these additional structures with the outcomes of quantitative comparisons cannot be excluded, the entorhinal cortex is the major constituent of the schizocortex. Also, the relation between indices for the hippocampus and schizocortex is very similar between bats and primates but differs from that of the rat. It is therefore not surprising that structural similarities exist in layer V of bats and primates. The cortical and sub-cortical inputs into layer V and intrinsic associational connections suggest that it may play a more significant role in memory operations (Burwell and Amaral 1998; Hamam et al. 2000, 2002; Kerr et al. 2007; Suzuki and Amaral 1994). At least for CA → entorhinal → cortical interactions bats may serve as a primate-like model.

If the morphology of layer II, which appears more rodent-like in structure, can be used as a guideline, this is not true for cortical → entorhinal → dentate interactions. However, EC layer II also differs between the two bats, and both bats apparently differ in the cellular composition and relative sizes of MEA layer II from primates and rodents (see below). We previously suggested that changes in the structure and connectivity of the phylogenetically rather pliable dentate gyrus may subserve species-specific demands on hippocampal function (Slomianka and Geneser 1991; Slomianka and West 1989). Species- and/or group-specific changes in the cortical region providing input to the dentate gyrus, as observed in the EC layer II of bats, should therefore be expected.

MEA layer II neuronal phenotypes and proportions

Cytoarchitectonic descriptions of the MEA in the rat (Insausti et al. 1997), mouse (Slomianka and Geneser 1991), dog (Woźnicka et al. 2006), macaque (Amaral et al. 1987), baboon (Blaizot et al. 2004) and human (Insausti et al. 1995) indicate that the stellate cell is the dominant neuronal phenotype. Quantitative studies estimated that stellate cells constitute 67–81% of the neuronal population and pyramidal cells between 16 and 32% in the rat and human MEA layer II (Mikkonen et al. 2000; Schwartz and Coleman 1981). We found that this layer contains an unusually large proportion of small cells (24 and 35%) that are neither stellate nor pyramidal. The stellate cell in the bats, as the single dominant phenotype at 36 and 41%, is well below reported values of over 60%. However, estimates of the pyramidal cell at ~18% are rather close to those of other species. Intracellular neuronal staining (Mikkonen et al. 2000) may have been biased by the selection of large cells in restricted EC areas, while Schwartz and Coleman (Schwartz and Coleman 1981) estimated proportions within only hippocampally projecting layer II cells. The number-weighted selection of cells for classification using disector probes at a uniform random systematic set of sampling sites throughout the EC should be unbiased by cell size and distribution. However, methodological differences cannot easily explain why one set of numbers is so different while another set is very close, and it is likely that bats differ from rats and humans in the cellular composition of MEA layer II. To pinpoint the nature of differences, a design-based stereological assessment of the cellular composition in the other species is needed.

Neuron number in the rat was estimated to 6.6×10^4 in MEA layer II (Mulders et al. 1997). This is almost twice the count in Wahlberg's epauletted fruit bat, which has approximately the same brain weight (2 g) as a rat, and although comparable to the straw-coloured fruit bat, the brain weight (4 g) is about twice that of the rat. It would be of interest to establish if the input from layer II is shared by the dentate gyrus and CA2/3 region of the hippocampus in the ratio (~17.7) reported in the primates and rat (Mulders et al. 1997). In the dentate gyrus, the straw-coloured fruit bat has an estimated mean total granule cell count of ~1,200,000 and that of Wahlberg's epauletted fruit bat is ~900,000 (C. Gatome, unpublished observations). The ratios granule cells:MEA layer II of ~19 (straw-coloured fruit bat) or ~29 (Wahlberg's epauletted fruit bat) show that large differences in the divergence of the projection

from the MEA layer II to the dentate gyrus can occur in closely related species. The estimated ratio in the rat of about ~18 (Mulders et al. 1997; West et al. 1991) distinctly differs from Wahlberg's epauletted fruit bat. This difference in divergence may well explain the increase in the size of some neuronal phenotypes, likely to be hippocampal projecting in Wahlberg's epauletted fruit bat, which is the smaller species.

Functional implications

Stellate cells are, in the entorhinal cortex as elsewhere, considered modified pyramidal cells (Germroth et al. 1989b, 1991; Klink and Alonso 1997a; Peters and Jones 1984) and share with them a number of electrophysiological properties (Alonso and Klink 1993; Alonso and Llinas 1989; van der Linden and Lopes da Silva 1998). However, the two cell types differ from their morphological complements in layer III (Erchova et al. 2004; van der Linden and Lopes da Silva 1998), and, for example, in their modulation by cholinergic inputs also from each other (Klink and Alonso 1997b). This may imply two parallel channels that act differently on the hippocampus (Alonso and Klink 1993; Klink and Alonso 1997a). The physiological properties of non-stellate or non-pyramidal neurons are not reported, although it is known that some phenotypes, such as the horizontal bipolar and tripolar cells also contribute to the perforant pathway (Germroth et al. 1989a).

The medial EC contains grid cells that fire selectively in specific locations in the environment (Brun et al. 2008; Fyhn et al. 2004; Hafting et al. 2005). Although correlational evidence based on dynamic membrane properties points towards the stellate cell as the anatomical equivalent of the grid cell (Garden et al. 2008; Giocomo and Hasselmo 2008), other morphological phenotypes cannot be ruled out. The current knowledge on grid cells supports a two-dimensional representation of the environment (Hafting et al. 2005). If and how grid cells represent dimensions that not only reflect movement across a surface but also above a surface is a question that, in mammals, can most easily be addressed in bats. It is tempting to speculate that the relative proportions of cell types within layer II are associated with the representation of a three-dimensional environment. Alternatively, the proportions observed in bats may be a trait reflecting the phylogenetic history of the Chiroptera, which must accommodate, but is not necessarily specific to a three-dimensional representation.

Acknowledgments We thank Prof. Menno Witter for a critical reading of the manuscript. We are grateful for the help of Mr. Ben Agwanda (National Museums of Kenya, Nairobi), and Dr. Robert Kityo (Makerere University, Kampala) for guidance on the species biology and ecology and logistical support, Mr. Francis Muchemi (National Museums of Kenya, Nairobi), and Dr. Joseph M. Bukenya (Rubaga Hospital, Kampala) for assistance in the capture. Dr. Urs Ziegler (ZMB, Zürich) kindly introduced us to the 3D modelling software. This work was supported by grants from Rita Levi Montalcini Fellowship for African Women in Neuroscience, International Brain Research Organisation, National Centre for Competence in Research (NCCR) Neural Plasticity and Repair, and Swiss National Science Foundation.

References

Alonso A, Klink R (1993) Differential electroresponsiveness of stellate and pyramidal-like cells of medial entorhinal cortex layer II. J Neurophysiol 70:128–143

Alonso A, Llinas RR (1989) Subthreshold Na^+-dependent theta-like rhythmicity in stellate cells of entorhinal cortex layer II. Nature 342:175–177

Amaral DG, Insausti R, Cowan WM (1987) The entorhinal cortex of the monkey: I. Cytoarchitectonic organization. J Comp Neurol 264:326–355

Ashwell KW, Zhang LL, Marotte LR (2005) Cyto- and chemoarchitecture of the cortex of the tammar wallaby (*Macropus eugenii*): areal organization. Brain Behav Evol 66:114–136

Baron G, Stephan H, Frahm HD (1996a) Atlases of a Megachiroptera brain. In: Baron G, Stephan H, Frahm HD (eds) Comparative neurobiology of Chiroptera: macromorphology, brain structures, tables and atlases, vol 1. Birkhäuser Verlag, Basel, pp 433–529

Baron G, Stephan H, Frahm HD (1996b) Comparative brain characteristics. In: Baron G, Stephan H, Frahm HD (eds) Comparative neurobiology of Chiroptera: macromorphology, brain structures, tables and atlases, vol 1. Birkhäuser Verlag, Basel, 529 pp

Beall MJ, Lewis DA (1992) Heterogeneity of layer II neurons in human entorhinal cortex. J Comp Neurol 321:241–266

Blaizot X, Martinez-Marcos A, Arroyo-Jimenez MdM, Marcos P, Artacho-Perula E, Munoz M, Chavoix C, Insausti R (2004) The parahippocampal gyrus in the Baboon: anatomical, cytoarchitectonic and magnetic resonance imaging (MRI) Studies. Cereb Cortex 14:231–246

Brodmann K (1909) Vergleichende Lokalisationslehre der Grosshirnrinde in ihren Prinzipien dargestellt auf Grund des Zellenbaues. Barth, Leipzig

Brodmann K (1925) Vergleichende Lokalisationslehre der Grosshirnrinde. C. G. Leipzig, Röder GmbH, pp 177–183

Brun VH, Solstad T, Kjelstrup KB, Fyhn M, Witter MP, Moser EI, Moser MB (2008) Progressive increase in grid scale from dorsal to ventral medial entorhinal cortex. Hippocampus 18:1200–1212

Buhl EH, Dann JF (1991) Cytoarchitecture, neuronal composition, and entorhinal afferents of the flying fox hippocampus. Hippocampus 1:131–152

Burwell RD, Amaral DG (1998) Perirhinal and postrhinal cortices of the rat: interconnectivity and connections with the entorhinal cortex. J Comp Neurol 391:293–321

Campbell MJ, Morrison JH (1989) Monoclonal antibody to neurofilament protein (SMI-32) labels a subpopulation of pyramidal neurons in the human and monkey neocortex. J Comp Neurol 282:191–205

DeFelipe J, Hendry SH, Jones EG (1989) Visualization of chandelier cell axons by parvalbumin immunoreactivity in monkey cerebral cortex. Proc Natl Acad Sci USA 86:2093–2097

Dorph-Petersen KA, Nyengaard JR, Gundersen HJG (2001) Tissue shrinkage and unbiased stereological estimation of particle number and size. J Microsc 204:232–246

Erchova I, Kreck G, Heinemann U, Herz AV (2004) Dynamics of rat entorhinal cortex layer II and III cells: characteristics of

membrane potential resonance at rest predict oscillation properties near threshold. J Physiol 560:89–110
Fonseca M, Soriano E, Ferrer I, Martinez A, Tunon T (1993) Chandelier cell axons identified by parvalbumin-immunoreactivity in the normal human temporal cortex and in Alzheimer's disease. Neuroscience 55:1107–1116
Frederickson CJ, Koh JY, Bush AI (2005) The neurobiology of zinc in health and disease. Nat Rev Neurosci 6:449–462
Fyhn M, Molden S, Witter MP, Moser EI, Moser M-B (2004) Spatial representation in the entorhinal cortex. Science 305:1258–1264
Fyhn M, Hafting T, Witter MP, Moser EI, Moser M-B (2008) Grid cells in mice. Hippocampus 18:1230–1238
Garden DL, Dodson PD, O'Donnell C, White MD, Nolan MF (2008) Tuning of synaptic integration in the medial entorhinal cortex to the organization of grid cell firing fields. Neuron 60:875–889
Geneser-Jensen FA, Haug FM, Danscher G (1974) Distribution of heavy metals in the hippocampal region of the guinea pig. A light microscope study with Timm's sulfide silver method. Z Zellforsch Mikrosk Anat 147:441–478
Germroth P, Schwerdtfeger WK, Buhl EH (1989a) GABAergic neurons in the entorhinal cortex project to the hippocampus. Brain Res 494:187–192
Germroth P, Schwerdtfeger WK, Buhl EH (1989b) Morphology of identified entorhinal neurons projecting to the hippocampus. A light microscopical study combining retrograde tracing and intracellular injection. Neuroscience 30:683–691
Germroth P, Schwerdtfeger WK, Buhl EH (1991) Ultrastructure and aspects of functional organization of pyramidal and nonpyramidal entorhinal projection neurons contributing to the perforant path. J Comp Neurol 305:215–231
Giocomo LM, Hasselmo ME (2008) Time constants of h current in layer ii stellate cells differ along the dorsal to ventral axis of medial entorhinal cortex. J Neurosci 28:9414–9425
Goldstein ME, Sternberger LA, Sternberger NH (1983) Microheterogeneity ("neurotypy") of neurofilament proteins. Proc Natl Acad Sci USA 80:3101–3105
Gundersen HJG, Jensen EB, Kiêu K, Nielsen J (1999) The efficiency of systematic sampling in stereology–reconsidered. J Microsc 193:199–211
Hafting T, Fyhn M, Molden S, Moser MB, Moser EI (2005) Microstructure of a spatial map in the entorhinal cortex. Nature 436:801–806
Hamam BN, Amaral DG, Alonso AA (2000) Morphological and electrophysiological characteristics of layer V neurons of the rat medial entorhinal cortex. J Comp Neurol 418:457–472
Hamam BN, Amaral DG, Alonso AA (2002) Morphological and electrophysiological characteristics of layer V neurons of the rat lateral entorhinal cortex. J Comp Neurol 451:45–61
Hassiotis M, Paxinos G, Ashwell KW (2004) Cyto- and chemoarchitecture of the cerebral cortex of the Australian echidna (*Tachyglossus aculeatus*). I. Areal organization. J Comp Neurol 475:493–517
Hassiotis M, Paxinos G, Ashwell KW (2005) Cyto- and chemoarchitecture of the cerebral cortex of an echidna (*Tachyglossus aculeatus*). II. Laminar organization and synaptic density. J Comp Neurol 482:94–122
Hendry SH, Jones EG, Emson PC, Lawson DE, Heizmann CW, Streit P (1989) Two classes of cortical GABA neurons defined by differential calcium binding protein immunoreactivities. Exp Brain Res 76:467–472
Hof P, Sherwood C (2005) Morphomolecular neuronal phenotypes in the neocortex reflect phylogenetic relationships among certain mammalian orders. Anat Rec A Discov Mol Cell Evol Biol 287A:1153–1163
Hof PR, Cox K, Morrison JH (1990) Quantitative analysis of a vulnerable subset of pyramidal neurons in Alzheimer's disease: I. Superior frontal and inferior temporal cortex. J Comp Neurol 301:44–54
Hof PR, Glezer II, Nimchinsky EA, Erwin JM (2000) Neurochemical and cellular specializations in the mammalian neocortex reflect phylogenetic relationships: evidence from primates, cetaceans, and artiodactyls. Brain Behav Evol 55:300–310
Holm IE, Geneser FA (1989) Histochemical demonstration of zinc in the hippocampal region of the domestic pig: I. Entorhinal area, parasubiculum, and presubiculum. J Comp Neurol 287: 145–163
Iñiguez C, Gayoso MJ, Carreres J (1985) A versatile and simple method for staining nervous tissue using Giemsa dye. J Neurosci Methods 13:77–86
Insausti R, Tuñón T, Sobreviela T, Insausti AM, Gonzalo LM (1995) The human entorhinal cortex: a cytoarchitectonic analysis. J Comp Neurol 355:171–198
Insausti R, Herrero MT, Witter MP (1997) Entorhinal cortex of the rat: cytoarchitectonic subdivisions and the origin and distribution of cortical efferents. Hippocampus 7:146–183
Jeffery KJ (2007) Integration of the sensory inputs to place cells: what, where, why, and how? Hippocampus 17:775–785
Johnson JI, Kirsch JA, Reep RL, Switzer RC 3rd (1994) Phylogeny through brain traits: more characters for the analysis of mammalian evolution. Brain Behav Evol 43:319–347
Jones G, Teeling EC (2006) The evolution of echolocation in bats. Trends Ecol Evol 21:149–156
Kerr KM, Agster KL, Furtak SC, Burwell RD (2007) Functional neuroanatomy of the parahippocampal region: the lateral and medial entorhinal areas. Hippocampus 17:697–708
Kingdon J (1984) Bats: fruit bats. In Kingdon J (ed) East African mammals: an atlas of evolution in Africa: Part A Insectivores and bats, vol 2. The University of Chicago Press, Hampshire, pp 117–174
Klink R, Alonso A (1997a) Morphological characteristics of layer II projection neurons in the rat medial entorhinal cortex. Hippocampus 7:571–583
Klink R, Alonso A (1997b) Muscarinic modulation of the oscillatory and repetitive firing properties of entorhinal cortex layer II neurons. J Neurophysiol 77:1813–1828
Kruska D (1975) Comparative quantitative study on brains of wild and laboratory rats. II. Comparison of size of allocortical brain centers. J Hirnforsch 16:485–496
Lapointe F, Baron G, Legendre P (1999) Encephalization, adaptation and evolution of chiroptera: a statistical analysis with further evidence for bat monophyly. Brain Behav Evol 54:119–126
Lorente de Nó R (1933) Studies on the structure of the cerebral cortex. J Psychol Neurol 45:381–438
Maseko BC, Manger PR (2007) Distribution and morphology of cholinergic, catecholaminergic and serotonergic neurons in the brain of Schreiber's long-fingered bat, *Miniopterus schreibersii*. J Chem Neuroanat 34:80–94
Maseko BC, Bourne JA, Manger PR (2007) Distribution and morphology of cholinergic, putative catecholaminergic and serotonergic neurons in the brain of the Egyptian rousette flying fox, *Rousettus aegyptiacus*. J Chem Neuroanat 34:108–127
Mikkonen M, Pitkänen A, Soininen H, Alafuzoff I, Miettinen R (2000) Morphology of spiny neurons in the human entorhinal cortex: intracellular filling with lucifer yellow. Neuroscience 96:515–522
Morrison JH, Lewis DA, Campbell MJ, Huntley GW, Benson DL, Bouras C (1987) A monoclonal antibody to non-phosphorylated neurofilament protein marks the vulnerable cortical neurons in Alzheimer's disease. Brain Res 416:331–336
Moser EI, Kropff E, Moser MB (2008) Place cells, grid cells, and the brain's spatial representation system. Annu Rev Neurosci 31:69–89

Mulders WH, West MJ, Slomianka L (1997) Neuron numbers in the presubiculum, parasubiculum, and entorhinal area of the rat. J Comp Neurol 385:83–94

O'Keefe J, Burgess N (2005) Dual phase and rate coding in hippocampal place cells: theoretical significance and relationship to entorhinal grid cells. Hippocampus 15:853–866

Paoletti P, Vergnano AM, Barbour B, Casado M (2009) Zinc at glutamatergic synapses. Neuroscience 158:126–136

Perez-Clausell J, Danscher G (1985) Intravesicular localization of zinc in rat telencephalic boutons. A histochemical study. Brain Res 337:91–98

Peters A, Jones EG (1984) Classification of cortical neurons. Classification of cortical neurons. In: Jones EG, Peters A (eds) Cerebral Cortex, vol 1. Plenum Press, New York, pp 107–121

Pettigrew JD, Jamieson BG, Robson SK, Hall LS, McAnally KI, Cooper HM (1989) Phylogenetic relations between microbats, megabats and primates (Mammalia: Chiroptera and Primates). Philos Trans R Soc Lond B Biol Sci 325:489–559

Pettigrew JD, Maseko BC, Manger PR (2008) Primate-like retinotectal decussation in an echolocating megabat, *Rousettus aegyptiacus*. Neuroscience 153:226–231

Pitkänen A, Amaral DG (1993) Distribution of parvalbumin-immunoreactive cells and fibers in the monkey temporal lobe: the hippocampal formation. J Comp Neurol 331:37–74

Ramón y Cajal S (1988) On a special ganglion of the spheno-occipital cortex. In: DeFelipe J, Jones EG (eds) Cajal on the cerebral cortex. An annoted translation of the complete writings. Oxford University Press, New York, pp 363–376

Rose M (1912) Histologische lokalisation der Grosshirnrinde bei Kleinen Saugetierein (Rodentia, Insectivora, Chiroptera). J Psychol Neurol 19:119–207

Rose M (1926) Der Allocortex bei Tier und Mensch. I. Teil. J Psychol Neurol 34:1–110

Rosene DL, Van Hoesen GW (1987) The hippocampal formation of the primate brain. A review of some comparative aspects of cytoarchitecture and connections. In: Jones EG, Peters A (eds) Cerebral cortex, vol 6. Plenum, New York, pp 345–456

Saleem KS, Price JL, Hashikawa T (2007) Cytoarchitectonic and chemoarchitectonic subdivisions of the perirhinal and parahippocampal cortices in macaque monkeys. J Comp Neurol 500:973–1006

Schwartz SP, Coleman PD (1981) Neurons of origin of the perforant path. Exp Neurol 74:305–312

Simmons NB, Seymour KL, Habersetzer J, Gunnell GF (2008) Primitive early Eocene bat from Wyoming and the evolution of flight and echolocation. Nature 451:818–821

Slomianka L (1992) Neurons of origin of zinc-containing pathways and the distribution of zinc-containing boutons in the hippocampal region of the rat. Neuroscience 48:325–352

Slomianka L, Geneser FA (1991) Distribution of acetylcholinesterase in the hippocampal region of the mouse: I. Entorhinal area, parasubiculum, retrosplenial area, and presubiculum. J Comp Neurol 303:339–354

Slomianka L, West MJ (1989) Comparative quantitative study of the hippocampal region of two closely related species of wild mice: interspecific and intraspecific variations in volumes of hippocampal components. J Comp Neurol 280:544–552

Slomianka L, West MJ (2005) Estimators of the precision of stereological estimates: an example based on the CA1 pyramidal cell layer of rats. Neuroscience 136:757–767

Stephan H, Baron G, Frahm HD, Stephan M (1986) Comparison of the size of brains and brain structures of mammals. Z Mikrosk Anat Forsch 100:189–212

Sternberger LA, Sternberger NH (1983) Monoclonal antibodies distinguish phosphorylated and nonphosphorylated forms of neurofilaments in situ. Proc Natl Acad Sci USA 80:6126–6130

Suzuki W, Amaral DG (1994) Topographic organization of the reciprocal connections between the monkey entorhinal cortex and the perirhinal and parahippocampal cortices. J Neurosci 14:1856–1877

Swanson LW, Cowan WM (1977) An autoradiographic study of the organization of the efferent connections of the hippocampal formation in the rat. J Comp Neurol 172:49–84

Swanson LW, Köhler C (1986) Anatomical evidence for direct projections from the entorhinal area to the entire cortical mantle in the rat. J Neurosci 6:3010–3023

Tandrup T (1993) A method for unbiased and efficient estimation of number and mean volume of specified neuron subtypes in rat dorsal root ganglion. J Comp Neurol 329:269–276

Teeling EC, Scally M, Kao DJ, Romagnoli ML, Springer MS, Stanhope MJ (2000) Molecular evidence regarding the origin of echolocation and flight in bats. Nature 403:188–192

Tuñón T, Insausti R, Ferrer I, Sobreviela T, Soriano E (1992) Parvalbumin and calbindin D-28K in the human entorhinal cortex. An immunohistochemical study. Brain Res 589:24–32

Ulanovsky N, Moss CF (2007) Hippocampal cellular and network activity in freely moving echolocating bats. Nat Neurosci 10:224–233

Uva L, Grüschke S, Biella G, De Curtis M, Witter MP (2004) Cytoarchitectonic characterization of the parahippocampal region of the guinea pig. J Comp Neurol 474:289–303

van der Linden S, Lopes da Silva FH (1998) Comparison of the electrophysiology and morphology of layers III and II neurons of the rat medial entorhinal cortex in vitro. Eur J Neurosci 10:1479–1489

van Groen T (2001) Entorhinal cortex of the mouse: cytoarchitectonical organization. Hippocampus 11:397–407

van Groen T, Miettinen P, Kadish I (2003) The entorhinal cortex of the mouse: organization of the projection to the hippocampal formation. Hippocampus 13:133–149

van Hoesen G, Pandya DN (1975) Some connections of the entorhinal (area 28) and perirhinal (area 35) cortices of the rhesus monkey. I. Temporal lobe afferents. Brain Res 95:1–24

West MJ, Slomianka L, Gundersen HJG (1991) Unbiased stereological estimation of the total number of neurons in thesubdivisions of the rat hippocampus using the optical fractionator. Anat Rec 231:482–497

Wouterlood FG, Hartig W, Bruckner G, Witter MP (1995) Parvalbumin-immunoreactive neurons in the entorhinal cortex of the rat: localization, morphology, connectivity and ultrastructure. J Neurocytol 24:135–153

Wóznicka A, Malinowska M, Kosmal A (2006) Cytoarchitectonic organization of the entorhinal cortex of the canine brain. Brain Res Rev 52:346–367